Nuclear-quadrupole induction of atomic polarization

Tycho Sleator and E. L. Hahn
Department of Physics, University of California, Berkeley, California 94720

Michael B. Heaney, Claude Hilbert, and John Clarke
Department of Physics, University of California, Berkeley, California 94720
and Materials and Chemical Sciences Division, Lawrence Berkeley Laboratory, Berkeley, California 94720
(Received 29 March 1988)

Nuclear-quadrupole-induced electric signals are measured as a new resonance response mechanism that is the reciprocal of the Stark effect in magnetic resonance. In single crystals that have noncentrosymmetry with respect to the sites of precessing nuclear-quadrupole moments, the electronic polarizability of atoms and chemical bonds on opposite sides of the nuclear-quadrupole moment is not the same. The oscillating electric field produced by the quadrupole moment induces a net electric dipole moment in its neighboring electronic environment. The coherent summation of these dipole moments over the Boltzmann distribution of the nuclear ensemble produces an oscillating macroscopic electric dipole moment. The sample is placed between the plates of a capacitor that is tuned with an inductance to the nuclear precession frequency. Coherent nuclear precession is initiated following a rf magnetic field pulse that tips the nuclear spins into the precession mode. The voltage signal from the capacitor gives rise to an oscillating current in the series circuit and magnetic flux in the inductor. Stray magnetic induction pickup signals are balanced out. The flux is coupled to a dc superconducting quantum interference device (SQUID), which produces a voltage output at the nuclear-quadrupole resonance frequency of ~ 30 MHz for ^{35}Cl nuclei in $NaClO_3$ at 4.2 K. The ^{35}Cl nucleus induces electric dipole moments in nearby oxygen atoms bonded to the Cl atom. Measured free-precession electric signals are compared to the predictions of a point-oxygen-atom polarizability model applied to the Cl—O bond. The technique is sensitive to chirality and to bond angles.

I. INTRODUCTION

In this investigation we present the results of an experiment that demonstrates the inverse or reciprocal property of the linear Stark effect in spin-resonance experiments. The linear Stark effect in electron spin paramagnetic resonance[1] (EPR) and in nuclear-quadrupole resonance[2] (NQR) results from the application of strong electric fields to spins located in noncentrosymmetric crystalline environments. Small frequency shifts of the spin-resonance frequency are observed with static electric fields, and oscillating electric fields applied at the appropriate spin transition frequencies produce absorption.[3] These measurements provide information on the crystal structure and a body of data for the analysis of chemical bond and atomic wave functions. Instead of measuring frequency shifts or absorption due to externally applied electric fields, we show that similar information is provided by means of a transient pulsed NQR method. A preliminary report[4] has been given of this method. The coherent emission of an electric signal is observed from the atomic polarization induced by an ensemble of precessing nuclear-quadrupole moments in a noncentrosymmetric crystal. This reciprocal method is free of effects which must be taken into account in the direct Stark experiment, where strong electric fields ($\sim 10^5$ V/cm) produce significant ion and bond angle displacements. These displacements must be included as corrections to the fundamental electronic polarization of bonds and atoms which we assume is the primary mechanism of the reciprocal Stark effect. In the radio-frequency range it will be shown (in contrast to EPR Stark absorption experiments)[1] that the reciprocal-pulse transient method[4] permits one to discriminate clearly against stray magnetic signals which may accompany and obscure the desired electric signals.

Oscillating electric signals derive from induced electric dipoles in atoms in the neighborhood of precessing nuclear-quadrupole moments. The summation of these induced moments over the sample results in a macroscopic polarization which induces a voltage on capacitor plates placed across the sample. The spin levels are first placed in coherent superposition by a rf magnetic field tipping pulse which couples to the nuclear magnetic moments. Following the pulse a free-induction-decay (FID) electric signal is emitted by the sample. The sample in the capacitor, which is part of a tuned *LCR* circuit, generates a current and therefore a flux which is inductively coupled to a dc SQUID (Ref. 5) (superconducting quantum interference device). In fact, if it were to be performed at higher temperatures the experiment would not necessarily require the high sensitivity of the SQUID. A rough estimate of the electric signal size using a "stick and ball" model is confirmed by our initial experiments, and shows that the signal from this effect is generally large enough to be detected by conventional amplifiers

and integration methods. The "stick" represents the distance **r** between a point "ball" nuclear quadrupole Q and the neighboring point "ball" atom which has polarizability α. The initial electric signal amplitude which directly follows the magnetic rf pulse is assumed to be a function of the coordinates of the polarizable atoms in the neighborhood of the nuclear quadrupole, the atomic polarizability α, and of the nuclear-quadrupole moment Q. These quantities **r**, α, and Q cannot be rigorously evaluated separately from the experimental data. Numerical estimates of these quantities combine to give a reasonable prediction of the measured signals. Although the mechanism of polarizability[6] is basic in modeling the reciprocal Stark effect, a more sophisticated wave-function analysis is necessary for rigorous treatment.

The electric signal amplitude can serve as an extra degree of freedom for the study of atomic motion in solids. At the same time, of course, the local motion of charges and atoms will produce small frequency fluctuations and possibly extra relaxation because of the electric quadrupole interaction. These effects are included in the FID decay envelope of the electric signal which is the same as that for the magnetic FID when both signals occur at the same frequency. Although the electric signal is generally smaller than the corresponding magnetic induction signal (by a factor 10^{-1}–10^{-3}, depending on the sample and nuclear quadrupole Q), the sensitive dependence of the electric signal amplitude on local lattice dynamics and structure should serve as a new and useful feature of the reciprocal Stark method.

II. THE ELECTRIC POLARIZATION FID SIGNAL

We first make a rough estimate of the signal-to-noise ratio expected from the experiment. A reciprocity relation will show that the electronic polarizability mechanism relates the direct Stark effect to our reciprocal experiment. The relation of the direct observation of nuclear-quadrupole radiation to our experiment is also outlined.

A. The electric signal-to-noise ratio

Our experiment is carried out with a single crystal of $NaClO_3$, where the ^{35}Cl nuclei exhibit a NQR precession frequency of $\omega_0/2\pi = 30.7$ MHz at 4.2 K. A rough estimate of the signal-to-noise power and voltage ratios is presented in this case. The precessing nuclear-quadrupole moment Q produces an electric field $\mathcal{E}_Q = eQS/r^4$ at a neighboring atom a distance r away. The Sternheimer[7] nuclear-quadrupole enhancement factor S has not been calculated for the Cl—O bond but is probably between 10 and 50. The net induced dipole moment is

$$p_0 = eQ\alpha S/r^4 \tag{1}$$

of magnitude $\approx 10^{-27}S$ esu cm. We have chosen the magnitudes $Q = 10^{-25}$ cm^2, $\alpha = 10^{-24}$ cm^2, and $r = 1.5$ Å (the Cl—O bond length in $NaClO_3$). The net induced macroscopic electric polarization is $P = N\beta p_0 \approx 1.6\times 10^{-9}S$ esu cm^2, where $N = 10^{22}$ atoms/cm^3 and the Boltzmann factor $\beta = \hbar\omega_0/2k_BT \approx 1.6\times 10^{-4}$ at $T = 4$ K for a two-level system. The voltage generated across the sample capacitance C_p is $V_s = PA_s/C$ where $A_s \approx 0.7$ cm^2 is the area of our 0.4-cm-thick sample placed between two metal plates. This capacitance is connected in parallel with a tuning capacitance C_t to give a total capacitance of $C = C_p + C_t \approx 10$ cm ≈ 10 PF. The average electric power dissipated in the circuit resistor R is therefore

$$P_s = V_s^2/2R = P^2A_s^2\omega_0Q_c/2C = 2\pi Q_c\omega_0P^2v_s\xi \ .$$

For the circuit quality factor $Q_c = 1/\omega_0RC \approx 1500$ in our experiments, $P_s \approx 1.8\times 10^{-15}S^2$ W. The volume of the sample is given by v_s and the sample filling factor is $\xi = \kappa A_s/4\pi dC \approx 0.014\kappa$ in our experiment, where d is the sample thickness and $\kappa = 5.4$ is the dielectric constant. Corrections due to modifications of P by the dielectric, and to fringe fields in C_p are neglected. The Nyquist noise power generated in R in a circuit bandwidth $B = 20$ kHz is $P_n = 4k_BTB \approx 4.4\times 10^{-18}$ W. Thus, given an amplifier with negligible noise, the electric signal-to-noise power ratio is $P_s/P_n \approx 2208S^2$, corresponding to a signal-to-noise current ratio of $I_s/I_n \approx 47S$. In our experiment the dc SQUID and post-amplifier contributed noise temperatures of about 0.5 and 1.5 K, respectively, so that the signal-to-noise ratio established by the Nyquist noise in R was not significantly degraded.

One may compare the electric power P_s with the optimized magnetic signal power[8] P_m obtained by placing the sample in the inductor. The expected emitted magnetic FID power is $P_m = 2\pi Q_c\omega_0M^2v_s\xi$, where $M = N\beta\mu$, ξ is the filling factor in the inductor, and v_s is the sample volume. For equivalent circuit parameters and signal integration in both experiments, the ratio of electric to magnetic powers becomes

$$P_s/P_m = p_0^2/\mu^2 \approx 10^{-6}S^2 \ , \tag{2}$$

where we have used $p_0 = 10^{-27}S$ and taken $\mu = 1$ nuclear Bohr magneton. Nuclear Sternheimer factors S range from about 1 to 100. The corresponding voltage ratio $(P_s/P_m)^{1/2} \approx 10^{-1}$–$10^{-3}$ implies that the electric signal relative to the magnetic signal is not necessarily very small in all cases. Even with the small filling factor of $\xi \approx 0.014\kappa$ applicable to the case of $NaClO_3$, the signal-to-noise ratio is quite generous, and could be increased several times by increasing ξ provided the total capacitance does not become so large that it lowers Q_c. Given these signal-to-noise ratio estimates it is quite feasible to consider the use of a conventional input amplifier in place of the SQUID.

B. The reciprocal Stark relation

In the direct NQR Stark effect the applied dc field E_l produces a shift component $\Delta q_{jk} = \Delta \mid \nabla\mathcal{E}_0 \mid_{jk}$ in the field gradient tensor at the position of the nucleus, where each of the j,k,l indices is any of the x,y,z directions. The nuclear-quadrupole Hamiltonian is given by

$$H_Q = H_Q^0 + H_Q'$$

where $\mathbf{Q}$ is the quadrupole tensor and $H_Q^0 = -\mathbf{Q}\cdot\nabla\mathcal{E}_0$. The perturbation H_Q' which corresponds to a frequency shift $\Delta\nu_{jk}$ may be written[2] as

$$|H_Q'|_{jk} \equiv h\Delta\nu_{jk} \equiv e^2 Q \sum_l R_{jkl} E_l \ , \tag{3}$$

where $R_{jkl} = \partial q_{jk}/\partial E_l$ is the tensor determined empirically in Stark shift experiments. Consider q charges in a single atom which has polarizability α characterized by ground- and excited-state energies W_0, W_i and ground- and excited-state wave functions $\langle 0|$ and $\langle i|$, respectively. The perturbation[2] in our model which may account for both absorption and frequency shifts is given by

$$H_Q' = \frac{\sum_q \sum_i \langle 0|H_Q^0|i\rangle\langle i|-e_q\mathbf{E}\cdot\mathbf{r}_{0p}|0\rangle}{W_i - W_0} + \text{H.c.} \ , \tag{4}$$

and is nonzero only in a noncentrosymmetric crystal where the $\langle 0|$ and $\langle i|$ states are of mixed parity. The applied electric field E may be constant or oscillating. The main quadrupole interaction H_Q^0 in Eq. (4) includes diagonal and off-diagonal operators, and may be expressed alternatively as

$$H_Q^0 = -\sum_q e_q\phi = -\sum_q e_q \mathbf{r}_{0p}\cdot\mathcal{E}_Q \ .$$

Here ϕ and $\mathcal{E}_Q = -\nabla\phi$ are respectively the potential and the electric field produced by the quadrupole Q at the position of a single polarizable point atom ("ball") which contains charges e_q. Therefore the final form of the perturbation may be written in operator form as

$$H_Q' = -\mathcal{E}_Q\cdot\vec{\alpha}\cdot\mathbf{E} \tag{5}$$

where $\alpha = \sum_q \sum_i e_q^2 \langle 0|r_{0p}|i\rangle\langle i|r_{0p}|0\rangle/(W_i - W_0)$ is the polarizability tensor, and $\mathcal{E}_Q$ depends upon quadrupole moment operators. The perturbation H_Q' can be expressed for N polarizable atoms as a dyadic macroscopic reciprocal relation

$$H_{Q\,\text{mac}}' = -N\beta v_s \mathcal{E}_Q\cdot\vec{\alpha}\cdot\mathbf{E} \tag{6a}$$

$$= -\mathbf{P}_Q\cdot\mathbf{E}v_s \tag{6b}$$

$$= -\mathbf{P}_E\cdot\mathcal{E}_Q v_s \tag{6c}$$

where $\mathbf{P}_Q = N\beta v_s\vec{\alpha}\cdot\mathcal{E}_Q$ and $\mathbf{P}_E = N\beta v_s\vec{\alpha}\cdot\mathbf{E}$. In our reciprocal experiment the quadrupole-induced oscillating polarization $\mathbf{P}_Q$ in Eq. (6b) automatically provides the reaction field $\mathbf{E} = -4\pi\mathbf{P}_Q$, which takes the place of an "oscillating applied field" $\mathbf{E}(\omega,t)$. With free precession $|\mathbf{P}_Q(t)| = P\cos(\omega t)$, the time derivative of (6b) results in the emitted free-precession electric power $P_s = 2\pi P_\omega^2 v_s \xi Q_c$ after one takes the time average and includes factors of Q_c and ξ. Consequently electric quadrupole coherent radiation damping occurs because an oscillating electric field gradient induces transitions toward the ground state to provide the power P_s. The reciprocal Stark relation (6a) therefore implies an electric field gradient perturbation Δq_{ij} at the site of the nuclear-quadrupole moment. This perturbation can be explicitly evaluated from the stick and ball model calculation, as discussed in Sec. VI.

C. Equivalence to detection of nuclear-quadrupole radiation

A sample of precessing nuclear-quadrupole moments contained in a quadrupole capacitor (two plates at right angles) will induce a direct oscillating electric quadrupole radiation signal across the plates. However, the expected signal is unobservably small,[9] of the order of 10^{-10} smaller than the corresponding NMR signal which would be obtained by placing the sample in an inductor. A direct experiment of this nature implies that one could observe the $\Delta m = \pm 2$ transitions directly corresponding to quadrupole moment operators $Q_2^{\pm 2}$. In effect the induced polarization experiment measures these transitions by using the local polarizability of atoms in the neighborhood of quadrupole moments to magnify the otherwise negligible direct quadrupole signal.

Consider a sample of n uniformly distributed precessing quadrupole moments eQ per unit volume. The resulting quadrupole moment density $\rho = neQ$ gives rise to a surface electric dipole moment density ρ, where the polarization $\mathbf{P} = \nabla\rho$, and therefore a potential drop $V = 4\pi\rho = 4\pi neQ$ occurs across the surface of the sample. If we now relate this potential drop to that discussed in Sec. II A, the induced polarization in our sample given by $P = np_0$ results in a voltage $V = 4\pi Pd = 4\pi n\alpha eQd/r^4$, where d is the thickness of the sample and p_0 is given by Eq. (1). Since the atomic polarizability α is on the order of an atomic volume, we take $\alpha \sim r^3$ and find $V \cong 4\pi neQ(d/r)$. With $d \sim 0.1$ cm and $r \sim 10^{-8}$ cm, this voltage is therefore on the order of $d/r \approx 10^7$ times larger than that achieved in the direct method imagined for observing nuclear-quadrupole radiation, and is sufficiently large for detection by the reciprocal Stark method.

III. EXPERIMENTAL CONFIGURATION

The configuration of the experiment is shown in Fig. 1(a). A rf pulse at the NQR frequency was coupled into a

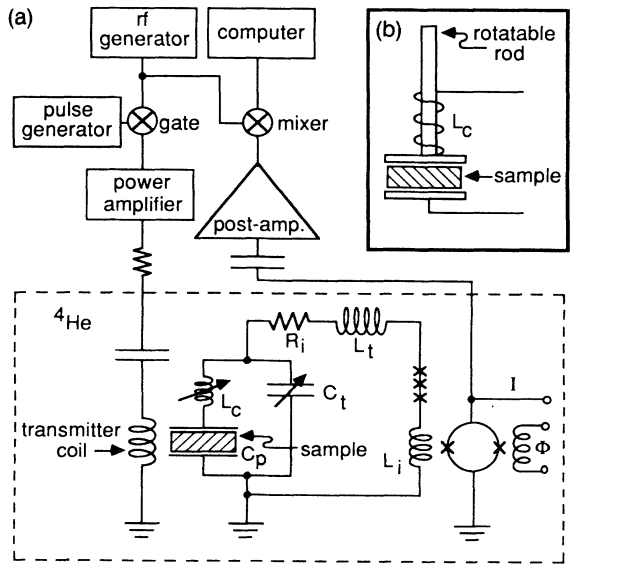

FIG. 1. (a) Experimental configuration. (b) Geometry of sample capacitor and cancellation coil.

cold transmitter coil in a Helmholtz arrangement. The pickup capacitor C_p containing the sample was centered in the transmitter coil with the plates perpendicular to the direction of the applied rf field $2H_1$, which we define as the laboratory x' axis. In addition to H_1, a small static magnetic field H_0 (ranging from 0 to about 10 G) was produced by a superconducting Helmholtz coil arrangement (not shown) and applied to the sample along the x' axis. The capacitor C_p, in parallel with a tuning capacitor C_t ($C_p+C_t=C$), was connected in series with an inductor L_t, an effective resistance R_i, the input coil L_i ($\ll L_t$) of a SQUID, and a series array of hysteretic Josephson tunnel junctions used[10] to protect the SQUID from the rf pulse and shorten the recovery time of the circuit. By adjusting C_t from the top of the cryostat we could tune the circuit to the NQR frequency. Current in the input circuit produced a flux through the SQUID loop and a voltage across the SQUID that was amplified by a room-temperature amplifier and mixed down with the signal from the rf generator. After the rf pulse was turned off, the mixed-down signal was recorded.

In addition to the induced electric signal P, the conventional NQR magnetic signal M is also present. The ratio of electric to magnetic signal powers $P_s/P_m<1$ expressed in Eq. (2) implies that a stronger magnetic signal is present at the same frequency as the electric signal. Unless one is careful to eliminate this stronger magnetic induction signal, it will be picked up by stray inductance and may dominate the electric polarization signal. The inductance L_c ($\ll L_t$), in series with C_p [Fig. 1(a)] and closely coupled to the sample, was used to pick up a magnetic induction signal and thereby to cancel the spurious signal [Fig. 1(b)]. By rotating a thin rod connected to the top plate of C_p, we could vary the number of turns of wire in L_c and cancel out the stray magnetic induction while leaving the electric signal unaffected. Details of the probe design are shown in Fig. 2.

Each sample was cut into a cylindrical shape 0.4 cm thick and 0.95 cm in diameter. We prepared two sets of samples, one with the crystal [100] direction along the cylindrical axis and the other with the [111] direction along the cylindrical axis. From NQR measurements in a weak static magnetic field,[11] we determined that the growth planes of the crystal are perpendicular to the three [100] directions. This information made it easy to position the crystal in the saw accurately (within a few degrees). Each crystal was irradiated with γ rays to reduce the spin-lattice relaxation time T_1 to about 2 min.

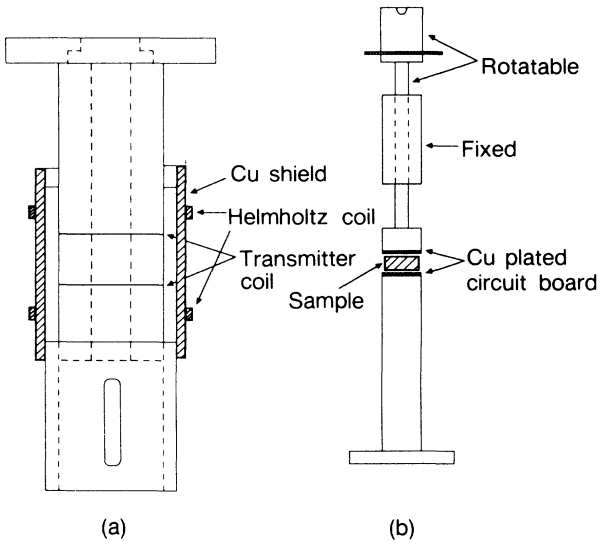

FIG. 2. Probe configuration of the quadruple-induced electric dipole experiment: (b) fits into (a).

IV. CALCULATION OF THE SIGNAL

The cancellation scheme discussed in the previous section is effective only if one can distinguish the electric polarization signal from the stray magnetic induction signal. In this section we make a detailed calculation of the expected electric polarization signal following the application of a rf magnetic field pulse. We assume that a small magnetic field H_0 is applied to the sample. We also derive expressions for the magnetic signal relevant to our experiment, following Bloom, Hahn, and Herzog.[11] It will be shown that the electric and magnetic signals have different modulation envelops in the presence of the field H_0 and can therefore be distinguished.

A. Outline of the calculation

Before proceeding with the calculation for the case of $NaClO_3$, an outline of the calculation is presented for an arbitrary quadrupole system in a solid.

(i) From the Hamiltonian, which may have both a quadrupolar part and a Zeeman part, we compute the spin states of the quadrupole nucleus for times after the rf pulse.

(ii) From these states, we calculate the expectation values of the various electric quadrupole moments $\langle Q_2^m \rangle$ using the convention

$$Q_2^0=[eQ/2I(2I-1)][3I_z^2-I(I+1)]\,,$$
$$Q_2^{\pm1}=\mp[\sqrt{6}eQ/4I(2I-1)](I_zI_\pm+I_\pm I_z)\,, \tag{7}$$
$$Q_2^{\pm2}=[\sqrt{6}eQ/4I(2I-1)](I_\pm)^2\,.$$

Henceforth the Sternheimer factor S is understood to be included in Q above, where $Q=Q_0S$ and Q_0 is the unshielded value of the quadrupole moment.

(iii) We determine the electric field $\mathcal{E}=-\nabla\phi$ (henceforth $\mathcal{E}$ is written in place of $\mathcal{E}_Q$) in the region surrounding the nuclear quadrupole from the value of $\langle Q_2^m \rangle$ using[12]

$$\phi(\eta)=(4\pi/5)^{1/2}(1/r^3)\sum_{m=-2}^{2}\langle Q_2^m\rangle Y_{2m}^*(\theta,\phi)\,, \tag{8}$$

where $\eta\equiv(r,\theta,\phi)$ is the position in local coordinates referred to an origin at the nuclear quadrupole.

(iv) We compute the total electric dipole moment $\mathbf{p}$ induced by a given nuclear quadrupole by summing the dipole moments $\mathbf{p}(\eta_i)$ induced on each atom over all the neighboring atoms, so that $\mathbf{p}=\sum_i \mathbf{p}(\eta_i)=\sum_i \alpha_i\mathcal{E}(\eta_i)$. It is assumed that the atoms are pointlike with polarizability α_i which is isotropic.

(v) The signal induced by each nucleus is summed over

all of the nuclei in the sample to yield the total electric polarization.

Note here that the conventional NMR signal M is determined by the expectation value of the operators $\mu_{\pm}=\gamma\hbar I_{\pm}$, which permit $\Delta m=\pm 1$ only. The induced electric polarization P, however, is determined by the expectation values of the quadrupole operators Q_2^m, which permit $\Delta m=0, \pm 1$, and ± 2.

B. Calculation of the nuclear-spin wave function

A unit cell of $NaClO_3$ is shown in Fig. 3. In the experiment, the Cl nucleus (spin $I=\frac{3}{2}$) is first prepared in a superposition state by the application of a rf field pulse defined by $H(t)=2H_1\cos(\omega t)$. During the short pulse of width t_w, where $1/t_w \gg \gamma H_0$, the Zeeman splittings caused by a small static magnetic field H_0 may be neglected, and therefore H_0 is omitted in the general Hamiltonian

$$H_Q=-\mathbf{Q}\cdot\nabla\mathcal{E}_0-\gamma\hbar\mathbf{I}\cdot[\mathbf{H}_0+\mathbf{H}(t)] ,$$

where $\nabla\mathcal{E}_0$ is the field gradient tensor at the site of Q. For long times $t>t_w$ the spin superposition states must take into account the Zeeman splittings by connecting amplitude coefficients of the spin wave functions directly after the pulse (when $H_0=0$) to those which include the Zeeman splittings (when $H_0\neq 0$).

The electric field gradient tensor is symmetric about the local z axis, which is along the direction of the Cl—Na bond. In the absence of the external magnetic field the eigenvalues are

$$W_m=-[e^2qQ/4I(2I-1)][3m_z^2-I(I+1)]$$
$$=\pm e^2qQ/4$$

for spin $I=\frac{3}{2}$. The eigenstates are $|m_z\rangle$, where m_z is the component of angular momentum along the z axis. The directions of H_0 and H_1 are defined by the angles θ_0, ϕ_0, and θ_1 as shown in Fig. 4. The x axis is chosen so that $\phi_1=0$ and lies in the plane determined by z and H_1.

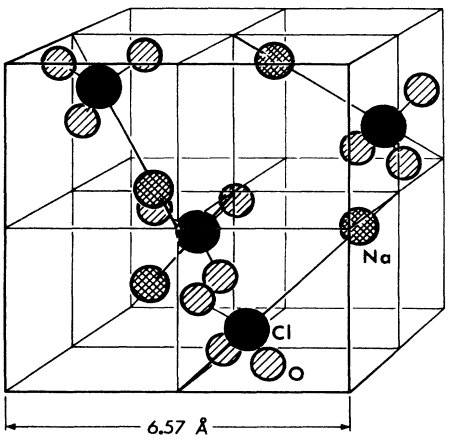

FIG. 3. Structure of a unit cell of $NaClO_3$.

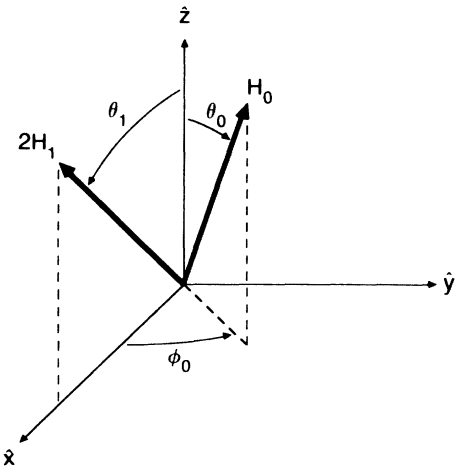

FIG. 4. Direction of H_0 and H_1 with respect to the local coordinates; $\hat{\mathbf{z}}$ is the local quantization axis and $\hat{\mathbf{x}}$ is chosen so that the azimuthal coordinate ϕ_1 for H_1 is zero.

In the presence of the field H_0 the eigenvalues and eigenstates are shown in Fig. 5. The wave function at any time can be expressed in the basis of angular momentum eigenstates

$$|\psi(t)\rangle=\sum_{m_z=-3/2}^{3/2} C_{m_z}(t)\,|m_z\rangle .$$

The wave function before the pulse ($t<0$) can be expressed by

$$C_{3/2}=1/\sqrt{2},\quad C_{-3/2}=e^{i\rho}/\sqrt{2},\quad C_{\pm 1/2}=0 ,$$

where ρ is the random phase factor over which one averages when computing expectation values. Immediately after the pulse

$$C_{m_z}(t_w)=C_{m_z}(0)\exp(-i\omega_{m_z}t_w) ,$$

where

$$C_{3/2}(0)=(1/\sqrt{2})\cos(2^{-1}\sqrt{3}\omega_1 t_w\sin\theta_1) ,$$

$$C_{1/2}(0)=(1/\sqrt{2})\sin(2^{-1}\sqrt{3}\omega_1 t_w\sin\theta_1) ,$$

$$C_{-3/2}(0)=e^{i\rho}C_{3/2}(0) ,$$

$$C_{-1/2}(0)=e^{i\rho}C_{1/2}(0) ,$$

with $\omega_1=\gamma H_1$. After the system has evolved for a time t (in the presence of H_0) we find

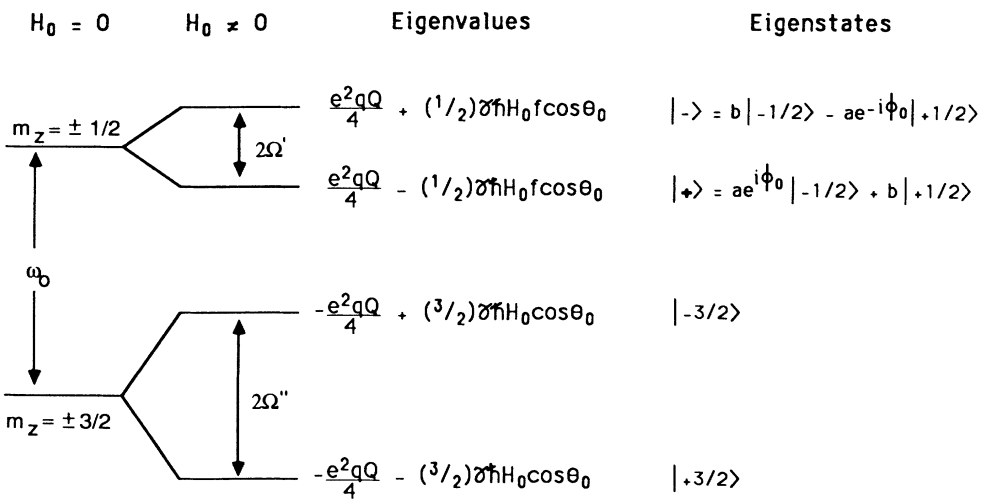

FIG. 5. Energy-level diagram for spin $I=\frac{3}{2}$ quadrupole interaction in a small magnetic field H_0. The parameters are $a=(\cos\theta_0/|\cos\theta_0|)[(f-1)/2f]^{1/2}$, $b=[(f+1)/2f]^{1/2}$, and $f=(1+4\tan^2\theta_0)$.

$$
\begin{aligned}
&C_{3/2}(t)=C_{3/2}(0)\exp(i\omega_0 t/2+i\Omega'' t)\ ,\\
&C_{-3/2}(t)=C_{-3/2}(0)\exp(i\omega_0 t/2-i\Omega'' t)\ ,\\
&C_{1/2}(t)=\exp(-i\omega_0 t/2)[(b^2e^{i\Omega' t}+a^2e^{-i\Omega' t})C_{1/2}(0)+2abi\exp(i\phi_0)\sin(\Omega' t)C_{-1/2}(0)]\ ,\\
&C_{-1/2}(t)=\exp(-i\omega_0 t/2)[(b^2e^{i\Omega' t}+a^2e^{i\Omega' t})C_{-1/2}(0)+2abi\exp(-i\phi_0)\sin(\Omega' t)C_{1/2}(0)]
\end{aligned}
\tag{9}
$$

where

$$
\begin{aligned}
&\omega_0=e^2qQ/2\hbar\ ,\\
&\Omega''=\tfrac{3}{2}\Omega_0\cos\theta_0\ ,\\
&\Omega'=\tfrac{1}{2}\Omega_0 f\cos\theta_0\ ,\\
&\Omega_0=\gamma H_0\ ,\\
&a=(\cos\theta_0/|\cos\theta_0|)[(f-1)/2f]^{1/2}\ ,\\
&b=[(f+1)/2f]^{1/2}\ ,\\
&f=(1+4\tan^2\theta_0)^{1/2}\ .
\end{aligned}
\tag{10}
$$

C. Calculation of the magnetic response from a single Cl nucleus

The expectation value of the magnetic moment $\boldsymbol{\mu}=\gamma\hbar\langle\mathbf{I}\rangle$ is evaluated from

$$\mu_+=\mu_x+i\mu_y=\gamma\hbar\langle\psi|I_+|\psi\rangle\ .$$

The result is

$$\mu_+=\sqrt{3}\gamma\hbar(C^*_{3/2}C_{1/2}+C^*_{-1/2}C_{-3/2})+2\gamma\hbar C^*_{1/2}C_{-1/2}\ .$$

We drop the term $2\gamma C^*_{1/2}C_{-1/2}$, which has low frequencies 0 and $2\Omega'$, because we are interested only in frequencies near ω_0. Evaluating the coefficients C_{m_z} we find

$$
\begin{aligned}
\mu_+=&(\sqrt{3}/2)\gamma\hbar\sin(\sqrt{3}\omega_1 t_w\sin\theta_1)[\sin(\omega_0 t)]\\
&\times[a^2\exp(-i\Omega_a t)+b^2\exp(-i\Omega_b t)]\ ,
\end{aligned}
$$

where

$$
\begin{aligned}
&\Omega_a=\Omega''+\Omega'=\tfrac{1}{2}\Omega_0(3+f)\cos\theta_0\ ,\\
&\Omega_b=\Omega''-\Omega'=\tfrac{1}{2}\Omega_0(3-f)\cos\theta_0\ .
\end{aligned}
\tag{11}
$$

Thus,

$$
\begin{aligned}
\boldsymbol{\mu}=(\sqrt{3}/2)\gamma\hbar W\{&[a^2\cos(\Omega_a t)+b^2\cos(\Omega_b t)]\\
&\times\hat{\mathbf{x}}-[a^2\sin(\Omega_a t)+b^2\sin(\Omega_b t)]\hat{\mathbf{y}}\}
\end{aligned}
\tag{12}
$$

where

$$W=\sin(\sqrt{3}\omega_1 t_w\sin\theta_1)\sin(\omega_0 t)$$

expresses the pulse "tipping angle" $\epsilon=\sqrt{3}\omega_1 t_w\sin\theta_1$.

D. Calculation of the quadrupole moments $\langle Q_2^m\rangle$

We now calculate the expectation values of the quadrupole moment operators Q_2^m, retaining only those terms with frequency near ω_0. From Eq. (3) we find

$$\langle Q_2^0\rangle=\frac{eQ}{2I(2I-1)}\langle\psi|3I_z^2-I(I+1)|\psi\rangle\ ,$$

which involves only terms with frequency 0 and $2\Omega'$;

$$\langle Q_2^1\rangle=\frac{-eQ}{2\sqrt{6}}\langle\psi\,|\,I_zI_+ +I_+I_z\,|\,\psi\rangle=-\langle Q_2^{-1}\rangle^*$$
$$=\frac{-eQ}{\sqrt{2}}(C^*_{3/2}C_{1/2}-C^*_{-1/2}C_{-3/2})$$
$$=\frac{-eQ}{2\sqrt{2}}i[a^2e^{-i\Omega_a t}+b^2e^{-i\Omega_b t}]R \tag{13}$$

and

$$\langle Q_2^2\rangle=\frac{eQ}{2\sqrt{6}}\langle\psi\,|\,I_+^2\,|\,\psi\rangle=\langle Q_2^{-2}\rangle^*$$
$$=\frac{eQ}{\sqrt{2}}(C^*_{3/2}C_{-1/2}+C^*_{1/2}C_{-3/2})$$
$$=\frac{-eQ}{\sqrt{2}}abR\,\sin(\Omega' t)\exp[-i(\Omega'' t-\phi_0)]\ , \tag{14}$$

where $R=\sin(\sqrt{3}\omega_1 t_w\sin\theta_1)\cos(\omega_0 t)$.

E. Computation of the electric field $\mathcal{E}$

At this point we divide the calculation into two parts by calculating the high-frequency responses from $\langle Q_2^{\pm1}\rangle$ and $\langle Q_2^{\pm2}\rangle$ separately. At position coordinates r,θ,ϕ the electric field $\mathcal{E}_1$ produced by $\langle Q_2^{\pm1}\rangle$ is obtained from Eq. (8) with $\Delta m_z=\pm1$:

$$\mathcal{E}_{1r}=(\tfrac{3}{2})^{1/2}\frac{3}{r^4}\sin\theta\cos\theta\langle Q_2'\rangle e^{-i\phi}+\text{H.c.}\ ,$$
$$\mathcal{E}_{1\theta}=-(\tfrac{3}{2})^{1/2}\frac{1}{r^4}(\cos^2\theta-\sin^2\theta)\langle Q_2'\rangle e^{-i\phi}+\text{H.c.}\ ,$$
$$\mathcal{E}_{1\phi}=(\tfrac{3}{2})^{1/2}\frac{i}{r^4}\cos\theta\langle Q_2'\rangle e^{-i\phi}+\text{H.c.}\ . \tag{15}$$

Equation (8) with $\Delta m_z=\pm2$ yields the electric field components produced by $\langle Q_2^{\pm2}\rangle$:

$$\mathcal{E}_{2r}=(\tfrac{3}{8})^{1/2}\frac{3}{r^4}\sin^2\theta\langle Q_2^2\rangle e^{-2i\phi}+\text{H.c.}\ ,$$
$$\mathcal{E}_{2\theta}=-(\tfrac{3}{8})^{1/2}\frac{2}{r^4}\sin\theta\cos\theta\langle Q_2^2\rangle e^{-2i\phi}+\text{H.c.}\ , \tag{16}$$
$$\mathcal{E}_{2\phi}=(\tfrac{3}{8})^{1/2}\frac{2i}{r^4}\sin\theta\langle Q_2^2\rangle e^{-2i\phi}+\text{H.c.}\ .$$

F. Computation of the electric polarization response for a single site

The electric dipole response $\mathbf{p}$ induced by a single Cl atom is $\mathbf{p}=\sum_i\alpha_i\mathcal{E}(\eta_i)$, where α_i is the polarizability of atom i located at position η_i relative to the Cl nucleus. Figure 6 shows the configuration of a single $NaClO_3$ molecule, giving the bond distances and angles. The angle δ shown in Fig. 6(b) is the angle that the Na-Cl-O plane makes with the Na-Cl-x plane. The angle δ depends on the direction of H_1 since the x axis is defined by the direction of H_1. Thus

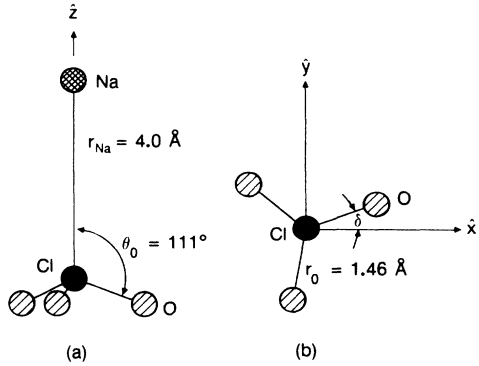

FIG. 6. Bond lengths and angles for a single molecule of $NaClO_3$: (a) side view, (b) view of ClO_3 ion from the $+\hat{\mathbf{z}}$ direction.

$$\phi_0=\begin{cases}\delta\\ \delta+2\pi/3\\ \delta+4\pi/3\ ,\end{cases}$$

where each term on the right refers to one of the three oxygen atoms in the ClO_3 group. All other neighboring atoms, including Na, are neglected since they are too far away to provide a significant contribution to $\mathbf{p}(\mathcal{E}\sim1/r^4)$. The polarizability of the oxygen atoms is not necessarily isotropic. One can deduce from the threefold symmetry of the ClO_3 group about the z axis that the polarizability α has a principle axis along $\hat{\boldsymbol{\phi}}$. If the other principle axes lie along $\hat{\boldsymbol{\theta}}$ and $\hat{\mathbf{r}}$, then $p_r(\eta_i)=\alpha_r\mathcal{E}_r(\eta_i)$, $p_\theta(\eta_i)=\alpha_\theta\mathcal{E}_\theta(\eta_i)$, and $p_\phi(\eta_i)=\alpha_\phi\mathcal{E}_\phi(\eta_i)$. Since α_r, α_θ, and α_ϕ are unknown, we assume for simplicity that the polarizability is isotropic and write $\mathbf{p}=\sum_i\alpha\mathcal{E}(\eta_i)$, where the summation is over the three oxygen atoms.

Before the various terms are summed, the dipole moment induced in each oxygen atom $p(\eta_i)$ is written in Cartesian coordinates as follows:

$$p_z(\eta_i)=p_r(\eta_i)\cos\theta-p_\theta(\eta_i)\sin\theta\ ,$$
$$p_x(\eta_i)+ip_y(\eta_i)=[p_r(\eta_i)\sin\theta+p_\theta(\eta_i)\cos\theta+ip_\phi(\eta_i)]e^{i\phi}\ . \tag{17}$$

(a) *Response from Q_2^1 term.* With $\mathcal{E}_i(\eta_i)$ from Eq. (15) and $\mathbf{p}(\eta_i)=\alpha\mathcal{E}(\eta_i)$ substituted into Eq. (17) one obtains

$$p_{1z}(\eta_i)=(\tfrac{3}{2})^{1/2}\frac{\alpha}{r^4}(5\cos^2\theta\sin\theta-\sin\theta)$$
$$\times\langle Q_2^1\rangle e^{-i\phi}+\text{H.c.}\ ,$$
$$p_{1x}(\eta_i)+ip_{1y}(\eta_i)=(\tfrac{3}{2})^{1/2}\frac{\alpha}{r^4}(5\sin^2\theta\cos\theta-2\cos\theta)$$
$$\times(\langle Q_2^1\rangle e^{-i\phi}+\text{H.c.})e^{i\phi}\ .$$

To sum the response we note that since the Cl-O azimuthal angles ϕ are at 120° with respect to one another,

$$\sum_i e^{\pm i\phi}=\sum_i e^{\pm2i\phi}=0$$

and

$$\sum_{i=1}^{3} 1 = 3 , \tag{18}$$

where the sum is taken over the positions of the three oxygen atoms to give the total polarizability $\mathbf{p}_i = \sum_{i=1}^{3} \mathbf{p}_i(\eta_i)$ with the components

$$p_{1z} = 0 ,$$
$$p_{1x} + ip_{1y} = 3\sqrt{3/2}\frac{\alpha}{r^4}(5\sin^2\theta\cos\theta - 2\cos\theta)\langle Q_2^1 \rangle . \tag{19}$$

We substitute $\langle Q_2^1 \rangle$ using Eq. (13) to give

$$p_{1x} + ip_{1y} = -ik_1 p_0 R\,[\,a^2\exp(-i\Omega_a t) + b^2\exp(-i\Omega_b t)] , \tag{20}$$

where, according to the parameters $\theta_0 = 111°$ and $r_0 = 1.5$ Å in Fig. 6,

$$k_1 = (3\sqrt{3}/4)(5\sin^2\theta_0\cos\theta_0 - 2\cos\theta_0) = -1.10$$

and

$$p_0 = eQ\alpha/r_0^4 .$$

The value of k_1 was computed using the value of $\theta_0 = 111°$ as shown in Fig. 6.

(b) *Response from Q_2^2 term.* We use Eqs. (16) and (17) with $\mathbf{p}(\eta_i) = \alpha\mathcal{E}(\eta_i)$ to find components

$$p_{2z}(\eta_i) = -(\tfrac{3}{8})^{1/2}\frac{\alpha}{r^4}5(\sin^2\theta)\cos\theta\langle Q_2^2 \rangle e^{-2i\phi} + \text{H.c.} ,$$

$$p_{2x}(\eta_i) + ip_{2y}(\eta_i) = -(\tfrac{3}{8})^{1/2}\frac{\alpha}{r^4}5\sin^3\theta \times(\langle Q_2^2 \rangle e^{-2i\phi} + \text{H.c.})e^{i\phi} .$$

Application to Eq. (18) and

$$\sum_i e^{i3\phi} = 3e^{i3\delta}$$

yields

$$p_{2z} = 0 , \tag{21}$$
$$p_{2z} + ip_{2y} = (\tfrac{3}{8})^{1/2}\frac{\alpha}{r^4}3e^{i3\delta}(-5\sin^3\theta)\langle Q_2^2 \rangle^* .$$

We substitute the quantity $\langle Q_2^2 \rangle^*$ given by Eq. (14) into Eq. (21), to find

$$p_{2x} + ip_{2y} = -ik_2 p_0 Rab \times\{\exp[i(\Omega_a t + 3\delta - \phi_0)] - \exp[i(\Omega_b t + 3\delta - \phi_0)]\} , \tag{22}$$

where

$$k_2 = (15\sqrt{3}/8)\sin^3\theta_0 = 2.64 .$$

It is interesting to compare the electric responses p_1 and p_2 [Eqs. (20) and (22)] with the magnetic response [Eq. (12)]. The magnetic moment μ is initially a maximum along the local x axis and appears to precess clockwise (if one looks down upon the xy plane for positive Ω_a, Ω_b). The electric polarizability p_1 also precesses clockwise but is initially a maximum along the local y axis. The polarizability p_2 is initially zero due to the cancellation of the frequency components Ω_a and Ω_b. However, each frequency component initially makes an angle of $3\delta - \phi_0$ with respect to the $\pm x$ axis and appears to precess in a counterclockwise direction.

G. Computation of the total electric response

To compute the total response of the sample we must sum the response for each molecule over all the molecules in a sample. A unit cell[13] (shown in Fig. 3) consists of four molecules of $NaClO_3$. The orientations of the four molecules can be specified in terms of the direction of the z axes relative to the crystal axes:

$$\mathbf{z}_1 = [1,1,1]/\sqrt{3},\quad \mathbf{z}_2 = [1,-1,-1]/\sqrt{3} ,$$
$$\mathbf{z}_3 = [-1,1,-1]\sqrt{3},\quad \text{and } \mathbf{z}_4 = [-1,-1,1]/\sqrt{3} .$$

The directions of the Cl—O bonds can be specified with a single parameter δ_0, the angle between the plane defined by $\mathbf{z}_1$ and the Cl(1)-O(1) direction and the plane defined by the directions $\mathbf{z}_1$ and $\mathbf{z}_2$. It is found that $\delta_0 = \pm 19.75°$ depending on whether the crystal is the "right-handed" isomer or the "left-handed" isomer (Fig. 7). In our experiments the fields H_0 and H_1 each point either along the laboratory x' axis or in the opposite direction. For the remainder of this calculation we assume that H_0 and H_1 point in the same direction (i.e., $\theta_0 = \theta_1$ and $\phi_0 = 0$) and along the x' axis. To consider the case where H_0 is reversed, we allow the magnitude of H_0 to be negative ($H_0 < 0$).

1. *Crystal (1,1,1) direction oriented along $\pm x'$*

The situation where the crystal [111] direction is pointing along the $\{\pm\}x'$ axis is shown in Figs. 8(a) and 8(b) for the two different sample orientations. First notice

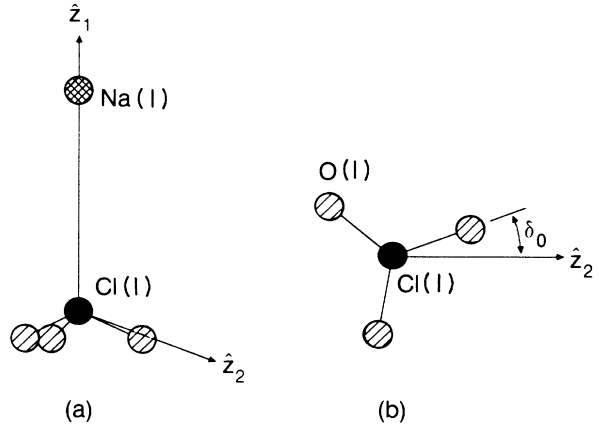

FIG. 7. Absolute orientation of $NaClO_3$ molecule: $\hat{\mathbf{z}}_1$ and $\hat{\mathbf{z}}_2$ are the quantization axes for two Cl atoms in a unit cell. (a) Side view, (b) view from the $+\hat{\mathbf{z}}_1$ direction. δ_0 is the angle between the Cl(1)—O(1) bond direction and $\hat{\mathbf{z}}_2$ projected onto the local x_1-y_1 planes.

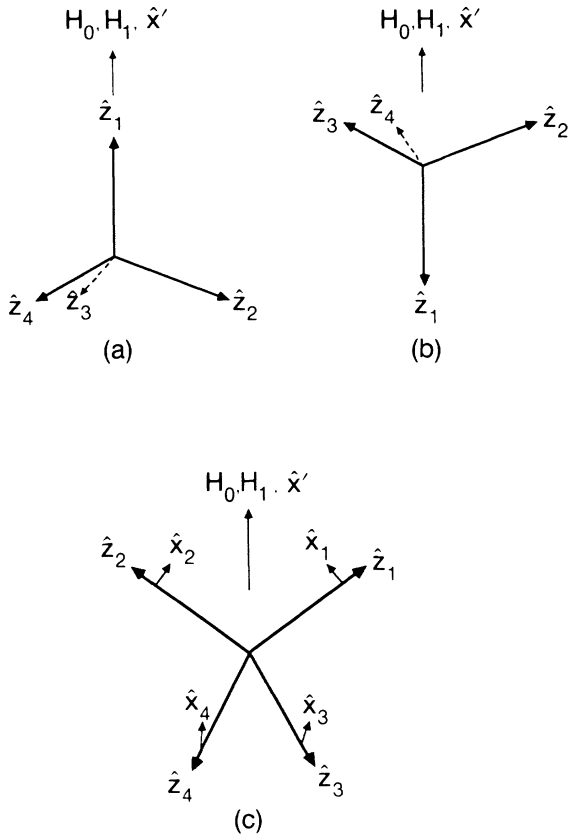

FIG. 8. Direction of local coordinate systems relative to the laboratory $\hat{\mathbf{x}}'$ axis for the crystal [111] direction along (a) $+\hat{\mathbf{x}}'$, and (b) $-\hat{\mathbf{x}}'$. (c) Direction of local coordinate systems relative to the laboratory $\mathbf{x}'$ axis for crystal [100] direction along $\hat{\mathbf{x}}'$.

that the site $\mathbf{z}_1$ produces no response since it is not affected by H_1 ($\theta_1=0$). The other three sites $\mathbf{z}_2$, $\mathbf{z}_3$, and $\mathbf{z}_4$ are all equivalent since they transform into each other upon a rotation about the [1,1,1] axis. For sites 2, 3, and 4, the various parameters are

$$\theta_0=\theta_1=\begin{cases}70.5^\circ\\109.5^\circ\end{cases},$$

$$\phi_0=0,\quad f=5.74,$$

$$a^2=0.413,\quad b^2=0.587,\quad ab=\{\pm\}0.492,$$

$$\Omega_a=\{\pm\}(1.46)\Omega_0,\quad \Omega_b=\{\pm\}(0.46)\Omega_0, \tag{23}$$

$$\delta_0=\langle\pm\rangle 19.75^\circ,$$

$$\delta=\begin{cases}\delta_0+\pi\\\delta_0\end{cases},$$

$$\cos 3\delta=\{\pm\}\cos 3\delta_0=\{\pm\}0.51,$$

$$\sin 3\delta=\{\pm\}\sin 3\theta_0=\{\pm\}\langle\pm\rangle 0.86.$$

The upper (lower) expressions in the braces { } correspond to [111] pointing along (against) $\hat{\mathbf{x}}$ (see Fig. 8). The upper (lower) expressions in the angular brackets $\langle\ \rangle$ refer to the right- (left-) handed enantiomer.

To sum the polarizations p resulting from all the Cl atoms in the sample we first sum over four sites in one unit cell. We note that

$$\sum_{i=1}^{4} p_{y_i}\hat{\mathbf{y}}_i = p_{y_1}\sum_{i=2}^{4}\hat{\mathbf{y}}_i = 0,$$

so that p_y does not contribute to the total response. The total response in the x direction for one unit cell is along the direction of H_1 and is

$$p_{\text{unit cell}}=(\sin\theta_1)\sum_{i=2}^{4} p_{x_i}=3(\sin\theta_1)p_x .$$

To obtain the total response from the sample we multiply this expression by the effective number of unit cells $\beta N/4$. In addition, we introduce a phenomenological damping factor $D(t)$ to account for spin-spin relaxation and inhomogeneous broadening,

$$P=P_1+P_2=\tfrac{3}{4}\beta N D(t)(\sin\theta_1)p_x=0.71\beta N(p_{1x}+p_{2x}).$$

Using Eqs. (20), (21), and (23) we find

$$P_1=-\beta N p_0 D(t)\sin(\sqrt{3}\omega_1 t_w\sin\theta_1)\cos(\omega_0 t)[0.32\sin(\Omega_a t)+0.46\sin(\Omega_b t)] \tag{24}$$

and

$$P_2=0.91\beta N p_0 D(t)R\{\cos(3\delta_0)[\sin(\Omega_a t)-\sin(\Omega_b t)]+\sin(3\Omega_0)[\cos(\Omega_a t)-\cos(\Omega_b t)]\} \tag{25}$$

$$=Np_0 D(t)\sin(\sqrt{3}\omega_1 t_w\sin\theta_1)\cos(\omega_0 t)$$
$$\times\{0.46[\sin(\Omega_a t)-\sin(\Omega_b t)]+\langle\pm\rangle 0.78[\cos(\Omega_a t)-\cos(\Omega_b t)]\}. \tag{26}$$

We follow similar arguments to find the total magnetic response

$$M(t)=\tfrac{3}{4}\beta N(\sin\theta_1)\mu_x$$

$$=-\beta N\gamma\hbar D(t)\sin(\sqrt{3}\omega_1 t_1\sin\theta_1)\sin(\omega_0 t)$$

$$\times[a^2\cos(\Omega_a t)+b^2\cos(\Omega_b t)]. \tag{27}$$

Figure 9 shows the plot for the particular combination $P(t)=1.2P_1-P_2$, where P_1 and P_2 are given by Eqs. (24) and (25). The reason for this combination, to be applied to our experimental results, will be given in Sec. V.

2. *Crystal [100] direction along x′*

The situation where the crystal [100] direction points along x' is shown in Fig. 8(c). Here, there are two sets of

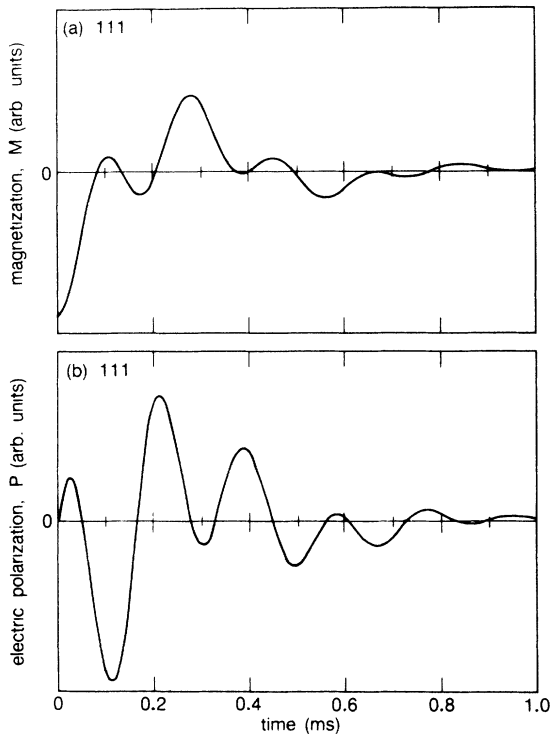

FIG. 9. Calculated free-induction signal response (arbitrary amplitude) for $H_0=8.8$ G in crystal [111] direction along $\hat{\mathbf{x}}'$: (a) magnetization $M(t)$, (b) electric polarization $P(t)$.

equivalent sites, those for which $\cos\theta_0>0$ (sites 1 and 2), and those for which $\cos\theta_0<0$ (sites 3 and 4). The values of the various parameters are as follows: $\theta_0=54.7°$ and $125.3°$ are the angles between x' and z_1,z_2 directions and z_3,z_4 directions, respectively;

$$\phi_0=0\ ,$$
$$f=3\ ,$$
$$a^2=\tfrac{1}{3},\quad b^2=\tfrac{2}{3},\quad ab=\{\pm\}\sqrt{2}/3\ ,$$
$$\Omega_a=\{\pm\}\sqrt{3}\Omega_0,\quad \Omega_b=0\ ,$$
$$\delta_0=\langle\pm\rangle 19.75°\ , \tag{28}$$
$$\delta_0=\begin{bmatrix}\delta_0\\ \delta_0+\pi\end{bmatrix}\ ,$$
$$\cos(3\delta)=\{\pm\}\cos(3\delta_0)=\{\pm\}0.51\ ,$$
$$\sin(3\delta)=\{\pm\}\sin(3\delta_0)=\{\pm\}0.86\ .$$

The upper term in the square brackets refers to sites 1 and 2, and the lower term refers to sites 3 and 4. We must sum over sites 1–4. Since $p_{y_1}=p_{y_2}$ and $p_{y_3}=p_{y_4}$ we find

$$\sum_{i=1,2} p_{y_i}\hat{\mathbf{y}}_i=0 \quad\text{and}\quad \sum_{i=3,4} p_{y_i}\hat{\mathbf{y}}_i=0\ ,$$

so there is no contribution from p_y. We also note that since $p_{x_1}=p_{x_2}$ and $p_{x_3}=p_{x_4}$ the total response for one unit cell (UC) is along the direction of H_1 and is

$$p_{UC}=(\sin\theta_1)\sum_{i=1}^{4} p_{x_i}\ .$$

There is no contribution from $Q_2^{\pm1}$ [Eq. (20)] since

$$\sum_i p_{x_i}=k_1p_0Ra^2\sum\sin(\{\pm\}\sqrt{3}\Omega_0t)=0\ .$$

The induced dipole moment is therefore given entirely by the $Q_2^{\pm2}$ term [Eq. (21)] as

$$p_{UC}=(\sin\theta_1)\sum k_2p_0Rab[-\sin(\Omega_at+3\delta)+\sin(3\delta)]$$
$$=(4.0)p_0R\sin(3\delta_0)[1-\cos(\sqrt{3}\Omega_0t)]\ , \tag{29}$$

where we have inserted the parameter values given in Eq. (28) and taken the sum over the four Cl atoms in a unit cell. The total polarization is

$$P(t)=-\langle\pm\rangle 0.86\beta Np_0D(t)\sin(\sqrt{3}\omega_1t_w\sin\theta_1)$$
$$\times\cos(\omega_0t)[1-\cos(\sqrt{3}\Omega_0t)]\ , \tag{30}$$

and the magnetic response for the [100] orientation is

$$M(t)=0.24\beta N\gamma\hbar D(t)\sin(\sqrt{3}\omega_1t_w\sin\theta_1)$$
$$\times\sin(\omega_0t)[2+\cos(\sqrt{3}\Omega_0t)]\ . \tag{31}$$

Both $P(t)$ and $M(t)$ for the [100] orientation are plotted in Fig. 10.

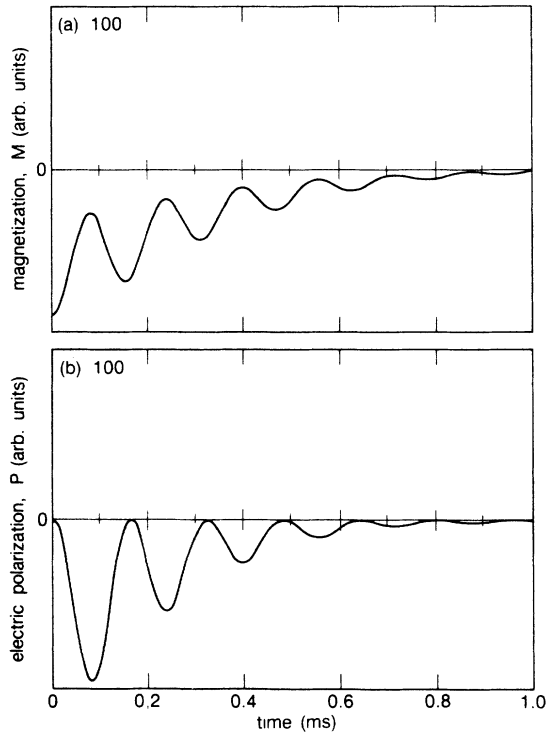

FIG. 10. Calculated free-induction signal response (arbitrary amplitude) for $H_0=8.8$ G in crystal [100] direction along $\hat{\mathbf{x}}'$: (a) magnetization $M(t)$, (b) electric polarization $P(t)$.

V. RESULTS AND DISCUSSION

We now compare the magnetic response M [Eqs. (27) and (31)] with the electric response P [Eqs. (24), (26), and (30)] and discuss whether they are in principle distinguishable. Common to both electric and magnetic signals is the term $\sin(\sqrt{3}\omega_1 t_w \sin\theta_1)$. The tipping angle $\epsilon=\sqrt{3}\omega_1 t_w \sin\theta_1$ reflects the degree to which the excited and ground states are mixed by the pulse. In addition, both electric and magnetic signals oscillate rapidly at frequency $\omega_0/2\pi$ (~ 30.7 MHz) indicated by the factor $\sin(\omega_0 t)$ in the magnetic signal and $\cos(\omega_0 t)$ in the electric signal. This difference in phase might lead one to think that the magnetic and electric signals could be selected individually by choosing the appropriate phase on the phase sensitive detector. This is not the case, however, because the coil that detects the magnetic signal differentiates the signal, giving it the same phase as the electric signal. In addition to an overall envelope decay in a time T_2 the rapidly oscillating electric and magnetic signals are modulated at frequencies Ω_a and Ω_b, which vary from 0 to 20 kHz in our experiments. It is this modulation envelope that allows one to distinguish the electric signal from the magnetic signal. For the case of the [111] direction along $\hat{\mathbf{x}}'$ [compare Eqs. (24) and (26) with Eq. (27)] and the case of the [100] direction along $\hat{\mathbf{x}}'$ [compare Eq. (30) and Eq. (31)], the modulation envelopes of the magnetic and electric signals are different. In addition, when $H_0=0$, Ω_a and Ω_b are also zero [see Eqs. (10) and (11)] and there is no electric signal, whereas the magnetic signal remains. For arbitrary crystal orientations there will in general be an electric response, even in the absence of the external magnetic field H_0.

The above results suggest the following experimental procedure. We choose a crystal orientation so that in the absence of an external static magnetic field there is no electric signal. Any signal that appears is therefore due to stray magnetic induction. One adjusts inductor L_c until the signal is reduced to zero, indicating the absence of magnetic pickup. We then apply the static magnetic field and record the mixed-down electric signal. The signal obtained by this procedure is shown in Fig. 11 for the [111] direction along $\hat{\mathbf{x}}'$ for $H_0=0$ to ± 13 G. Figure 11(a) shows the result of balancing out the magnetic signal in zero field (note that a very small magnetic signal remains). Also shown in Figs. 11(a)–11(i) are fits to the data using Eqs. (24) and (26) for P_1 and P_2. To make the fit we first determined the function $D(t)$ by the empirical fit of a magnetic induction signal $D(t)$ in zero field $H_0=0$ to that shown in Fig. 12(c). With this empirical determination of $D(t)$ we varied H_0 and the overall amplitudes of P_1 and P_2 to make the fit to the data. The values of Ω_a and Ω_b are determined by H_0 but the ratio Ω_a/Ω_b is fixed by the theory. Although our model predicts the electric signal should be given by $P=c_1P_1+c_2P_2$, where the parameter ratio $c_1/c_2=+1$, we measure the best fit to be obtained for $P=1.2P_1-P_2$ and $c_1/c_2=-1.2$. We will discuss possible explanations for this discrepancy after presenting the remaining data. The good quality of the fits obtained with these parameters (involving H_0 field reversals and variations in magnetic signal leakage) gives the correct functional form of the polarization induced by $Q_2^{\pm 1}$ and $Q_2^{\pm 2}$ but not the correct amplitudes.

Figure 13 shows the signal obtained with three different values of the inductive coupling for $H_0=0$ and $H_0=8.8$ G. The total signal $\mathcal{S}$ can be written as $\mathcal{S}=U(\text{magnetic signal})+V(\text{electric signal})$ for some constants U and V. As the amount of inductive coupling is changed, we expect the amount of magnetic signal U to vary but the amount of electric signal V to remain fixed. To make the fits to Fig. 12 we first determined the amount of magnetic signal by fitting the signal in zero field (left figures). With this amount of magnetic coupling, we adjusted the amount of electric signal to produce the best fit (right figures). While the amount of magnetic signal U varied from $+7$ units to -95 units (scale arbitrary), the amount of electric signal V varied by about 20%. The variation in V may have been due to a slight change in the electric coupling, since the adjustments of the inductor L_c causes the top plate of the pickup capacitor to rotate slightly. Alternatively, it is possible that a change in the gain of the system occurred during the time required for adjustment. By comparing Fig. 12(c) with Fig. 9(a) we see that even with the large magnetic coupling the electric signal still makes a significant contribution to the overall signal.

When H_0 is reversed, the signal changes its shape (Fig. 13). This same change in shape would occur if, instead of reversing H_0, the sample were flipped 180° about an axis perpendicular to $\hat{\mathbf{x}}'$, as one can prove using the definitions $\Omega_a=\{\pm\}(1.46)\gamma H_0$ and $\Omega_b=\{\pm\}(0.46)\gamma H_0$ [Eq. (23) and Eqs. (24) and (26)]. However, one can show in general for any sample orientation that the electric signal obtained after reversing H_0 is the same as the signal obtained after flipping the sample 180° about an axis perpendicular to $\hat{\mathbf{x}}'$.

If one knows the sample orientation and the direction of H_0, one can distinguish the two possible enantiomorphs of the sample. For example, if we assume that both H_0 and the [111] direction point along $+\hat{\mathbf{x}}'$ then both Ω_a and Ω_b are positive in Eq. (26). A fit of the data would yield the relative sign ($\{\pm\}$) of the two terms on the right side of Eq. (26) and therefore identify the enantiomorph.

The experiment was also performed with the sample [100] direction along $\hat{\mathbf{x}}'$, and the results are shown in Fig. 14 for several values of H_0. In this case we expect no contribution from Q_2^1, as discussed in Sec. III G b. A visual inspection indicates that the calculated signal $-D(t)[1-\cos(\sqrt{3}\Omega_0 t)]$ fits the data fairly well. When $\Omega_0=\gamma H_0$ is reversed, however, the measured signal undergoes a slight phase shift as indicated in Fig. 14, which is not predicted by the theory. We have already stated that reorientation of the sample 180° about an axis perpendicular to $\hat{\mathbf{x}}'$ is equivalent to reversing the direction of H_0. Since the $[\bar{1}00]$ direction is equivalent to the [100] direction, such a reorientation can have no influence on the signal. Therefore a reversal of the direction of H_0 can have no effect on the signal. However, a small phase shift did appear due to imperfect alignment of the sample or of the fields H_1 and H_0. This shift was easily incorporated into the fits by adding a small term proportional

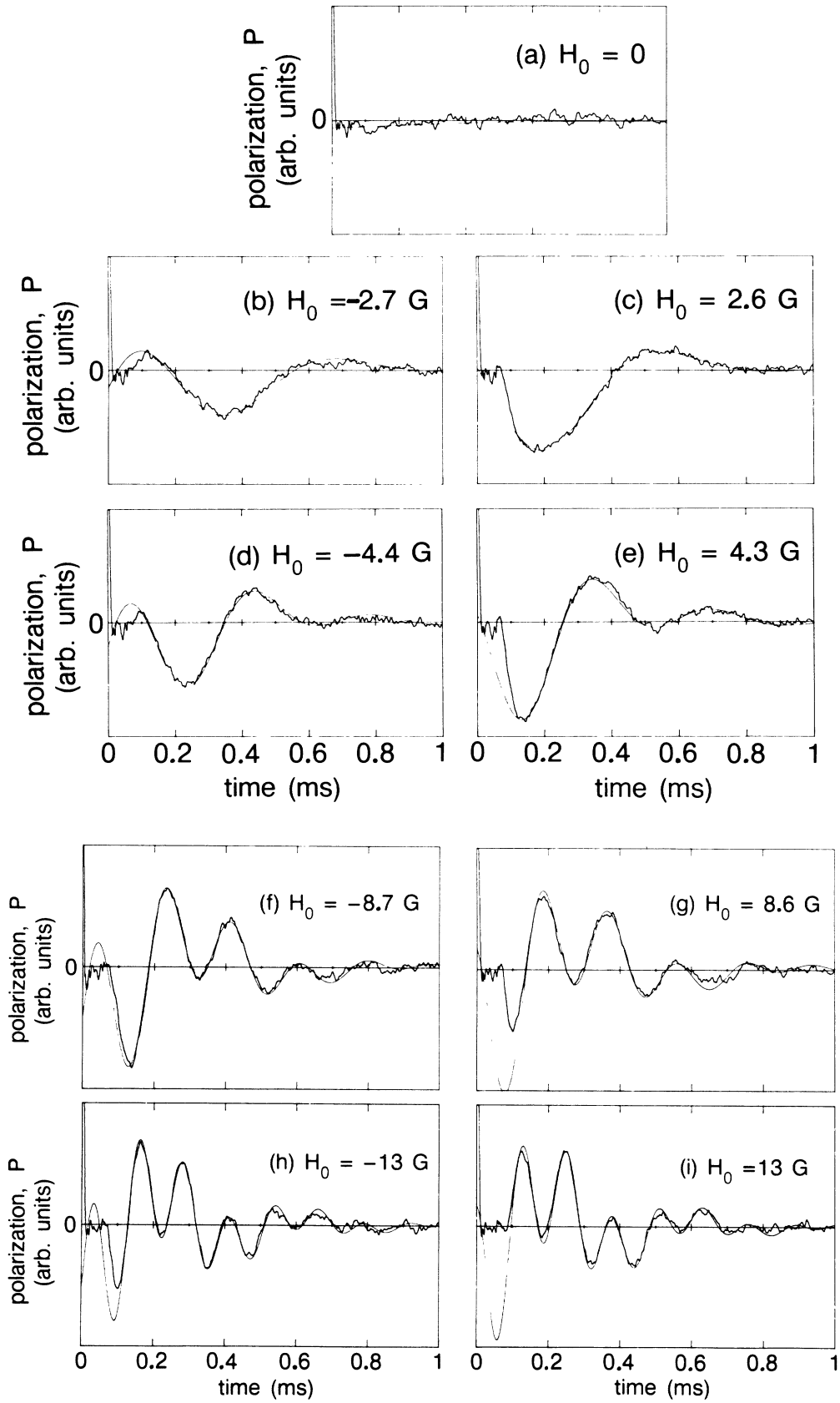

FIG. 11. Measured polarization signal envelope for the crystal [111] direction along $\hat{\mathbf{x}}'$ for different values of H_0. Smooth curves shows fits to $P(t)=1.2P_1-P_2$, Eqs. (24) and (26). At $H_0=0$ the magnetization pickup signal is balanced out. For times ≤ 0.1 ms the circuit is recovering from the rf pulse.

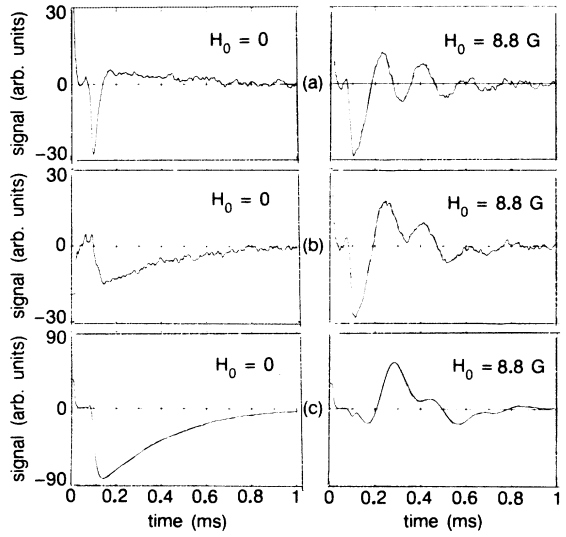

FIG. 12. Signal for sample [111] direction along $\hat{\mathbf{x}}'$ for three values of magnetic coupling.

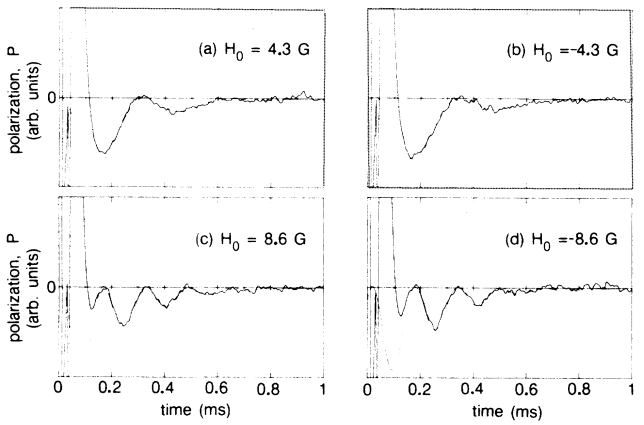

FIG. 14. Measured polarization signal envelopes for the crystal [100] direction along $\hat{\mathbf{x}}'$ for several values of H_0. Smooth curves show fits to $P(t)$ given by Eq. (30). For times $\lesssim 0.15$ ms the circuit is recovering from the rf pulse.

to $\sin(\sqrt{3}\Omega_0 t)$. These fits are shown in Fig. 14. The only fitting parameter varied when we obtained the data in Figs. 14(a)–14(d) was the value of H_0. An examination of Eq. (30) indicates that for the crystal [100] direction along $\hat{\mathbf{x}}$ one can in principle distinguish the two possible enantiomorphs of the sample. To make this distinction, however, one must be able to determine the phase of the signal (at ω_0) relative to the phase of the applied rf pulse. One can measure this phase by comparing the signal to a magnetic induction signal picked up by a coil with known helicity.

The experimental plots which compare to theoretical curves in our discussion result from free-induction signals induced in a tuned circuit, with response time of the circuit limited by the high figure of merit $Q \approx 1000$–2000. In addition, a slight misalignment of the $NaClO_3$ crystal mixes in most importantly a very small phase distortion of the expected signal. Therefore Figs. (11)–(14) show plots of theory curves [linear combinations of $P(t)$ and $M(t)$] which are slightly shifted in phase to fit the experimental curves, amounting to time delays of about 0.01 to 0.02 ms.

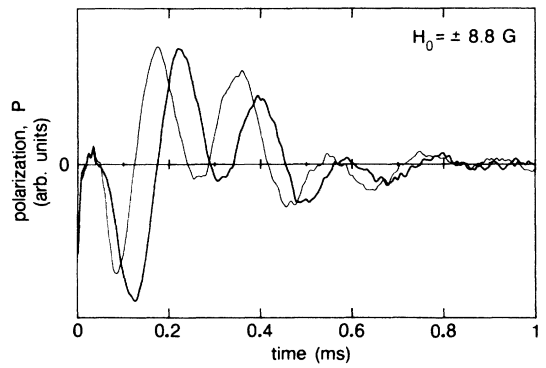

FIG. 13. Effect of static field reversal on electric polarization signal for crystal [111] direction along $\hat{\mathbf{x}}'$.

We now return to the discussion of the discrepancy between theory and experiment in the relative amplitudes of P_1 and P_2 for the case of the [111] orientation. In our calculation we have assumed that the atomic polarizability is isotropic. A generalization of the theory to include anisotropic polarizabilities affects the relative contributions to Q_2^{+1} and $Q_2^{\pm 2}$ but not to a sufficient degree to account completely for the discrepancy. Let us consider the very unlikely possibility that in our sample the oxygen atoms are rotated 60° about the Cl—Na bond from the positions given by the x-ray data[13] (i.e., $\delta_0 \rightarrow \delta_0 + 60°$). Under this transformation, $\cos(3\delta_0)$ and $\sin(3\delta_0)$ become $-\cos(3\delta_0)$ and $-\sin(3\delta_0)$ and the sign of P_2 in Eq. (25) changes, removing the discrepancy. The above scenario, presumably fictitious, gives one an idea of the sensitivity of the signal to the polarizable environment of the quadrupole nuclei. One must realize that our calculation was based on a model in which the atoms are located at discrete points. A correct calculation of the signal requires a model that properly takes into account the electronic wave functions of the ClO_3^- ion.[6] There is no reason to believe that the polarizable environment of the Cl nucleus described by the "ball and stick" model is the same as that described by the electronic wave functions. For example, since $\mathcal{E} \sim 1/r^4$ we expect the polarizable environment close to the Cl nucleus to dominate the signal. On this basis the direction and magnitude of maximum polarizability in the region close to the Cl nucleus may differ from that in the direction of the Cl—O chemical bond. In view of the absence of a rigorous quantum-mechanical analysis, one is restricted to using the polarizability model to account for the discrepancy in the [111] crystal orientation data.[14]

We can estimate the induced dipole moment p_0 from the data. Since the induced voltage across the total capacitance is $V = PA_s/C$, we find

$$P = I/A_s Q_c \omega_0 .$$

The current in the circuit $I = V/R_i$ is determined from the SQUID calibration, and $Q_c = 1/R\omega_0 C$ is determined from the ring-down time of the circuit, as described in the Appendix. For a tipping angle $1.4\omega_0 = 6\times 10^{-2}$, using Eq. (29) and the data in Fig. 14 we find $p_0 = 3\times 10^{-27}$ esu cm, an order-of-magnitude agreement with our *a priori* estimate provided $S \approx 1-50$.

In our experiment the choice of special crystal orientations to cancel out stray magnetic signals appears to be a difficult requirement. In principle if the theory is known for both electric and magnetic signal shapes, a fit of the data to the theory can be carried out without the need for canceling the stray magnetic signal. However, one cannot rely entirely on the theory using the stick and ball polarization model, as found in our measurements of $NaClO_3$ for the (111) orientation. If it were possible for the sample to contain a known concentration of spins with $I = \frac{1}{2}$, the magnetic signal from the precession of these spins could serve to correct for the stray pickup in the electric experiment. In a proposed electric experiment (see Sec. VII), in systems involving two photon transitions between states nominally separated by $\Delta m = \pm 2$, the magnetic rf excitation of any allowed $\Delta m = \pm 1$ transitions (because of neighboring state admixtures) can provide magnetic signals for calibration of stray magnetic pickup.

VI. STARK EFFECT BY EXTERNAL FIELDS

According to Eqs. (5) and (6) the induced electric dipole model may be applied to estimate the effect of an externally applied E field on the quadrupole resonance. An oscillating field $E(\omega,t)$ applied at the quadrupole transition frequency ω will induce atomic dipole moments in the neighborhood of nuclear-quadrupole moments Q. Oscillating electric field gradients from these induced dipoles in turn will induce quadrupole transitions. Alternatively it is convenient to express the quadrupole interaction in terms of applied field components which couple at resonance with "oscillating" atomic electric dipole moments p_{lm} induced by nuclear-quadrupole components Q_m^2. These dipole components may be evaluated explicitly from Eqs. (19) and (21) in the calculation for $NaClO_3$ as $p_{lm} = R_l^m Q_2^m$. Here $l = x,y,z$ refer to the quadrupole coordinate frame, $m = \pm 1, \pm 2$, with Q_2^m retained here in operator form, and R_l^m is the corresponding coefficient. Thus for a single Cl-O interaction the perturbation may be written in a form similar to Eq. (3) as

$$H_Q' = e \sum_l \sum_m R_l^m Q_2^m E_l(\omega,t) \ .$$

According to Eq. (3) we may define $\Delta q_{2m}(\omega,t) = R_l^m E_l(\omega,t)$ as the oscillating electric field gradient at the site of the quadrupole moment, which is produced by the induced dipole moment P_{lm}.

Nuclear-quadrupole frequency shifts occur for constant applied E fields, in which case the $m = 0$ index must be included above. As an example in which only $m = 0$ applies, consider an external field $E_z = E_0$ applied parallel to the quadrupole axis of symmetry in the direction of the Na→Cl bond. The frequency shift $\Delta\nu$ may be estimated for the zero-field ($B = 0$) transition $\Delta m_z = \pm\frac{1}{2} \leftrightarrow \pm\frac{3}{2}$ using the formalism of Eq. (5). For a single Cl—O bond

$$|H_Q'| = \frac{e\alpha Q_2^0 S}{2r^4}(\mathbf{E}_r + \mathbf{E}_\theta)\cdot\nabla\frac{1}{r^3}(3\cos^2\theta - 1) \ ,$$

where $E_\theta = -E_0 \sin\theta$, $E_r = E_0\cos\theta$, Q_2^0 is given in Eq. (7), and we assume the polarizability α is isotropic. After summing over three equivalent oxygen atoms, the difference in $|H_Q'|$ for Q_2^0 ($m = \pm\frac{3}{2}$) and Q_2^0 ($m = \pm\frac{1}{2}$) gives a positive frequency shift

$$\Delta\nu = \frac{9e\alpha Q_0 E_0 S}{2\hbar r^4}(5\cos^2\theta - 3)\cos\theta = 1.9S \ ,$$

in which we use the parameters for $NaClO_3$ applied earlier, and take $E_0 = 1000$ V/cm. The choice of $S \approx 50$ as a reasonable value of the Sternheimer factor yields $\Delta\nu \approx 100$ s^{-1}/kV as an estimate close to the value which has been observed.[2]

VII. FUTURE DIRECTIONS AND CONCLUSIONS

As stated previously the observation of the quadrupole-induced electric dipole does not necessarily require a dc SQUID at liquid-helium temperatures. If we were to perform the experiment at liquid-nitrogen temperature ($T = 77$ K) using a low-noise room-temperature amplifier with a noise temperature of about 100 K, the signal power would be reduced from that of our experiment by a factor $(\frac{4.2}{77})^{-2} \approx 400$, and the noise power would increase by the factor $\frac{100}{4.2} \approx 25$. The signal-to-noise ratio would therefore be about 10^4 less in power than that in our experiment for a single pulse of the same tipping angle. Given, however, that T_1 for $NaClO_3$ (≈ 1 s) at 77 K is 10^3 times shorter than the T_1 (≈ 20 min) at 4.2 K, the signal-to-noise ratio per unit time would be reduced from the value in our experiments by only a factor of 10 in power, or a factor of 3 in voltage (in this estimate we have not considered the lower Q or increased losses that would occur at liquid-nitrogen temperatures). The ability to perform the measurement at liquid-nitrogen temperature is important for samples where T_1 at 4.2 K is so long that it would be impossible to perform the experiment.

We now discuss two possible extensions of our experiment. One variation would be to observe the electric signal from a system with spin $I > \frac{1}{2}$ in a high magnetic field H_0 ($\gamma\hbar H_0 \gg eqQ$), where the levels are unequally spaced. After a rf pulse is applied at a frequency ω_0, exciting a two photon transition,[15] the superposition of states separated by $\Delta m = \pm 2$ results in a quadrupole-induced electric signal of the form $Q_2^{\pm 2}$ at frequency $2\omega_0$. Hence one avoids the stray magnetic induction signal at ω_0 (corresponding to $\Delta m = \pm 1$), and is required to cancel out a very small contribution at $2\omega_0$ arising from state mixing. The relaxation times T_1 and T_2 of the electric signal would be different from the relaxation of the magnetic FID signal which pertains to $\Delta m = \pm 1$ transitions.

For the second extension, we note that since the capacitor containing the sample is part of a tuned circuit, the electric polarization signal results in dissipation of energy

in the resistor R_i in the circuit as pointed out in Sec. II B. This loss of energy from the spins must be accompanied by nuclear-spin transitions from the excited state to the ground state. These transitions must be due to the back-reaction of the circuit by means of an oscillating electric field across the sample. Just as this electric field causes transitions by polarizing atoms in the sample, one could in turn apply oscillating electric field gradients indirectly to the quadrupoles as discussed in Sec. VI. A pulsed "reciprocal" experiment is possible in which one applies an electric field at ω_0 (or $2\omega_0$), inducing quadrupole transitions. After the electric pulse these transitions may be monitored by observing a magnetic induction signal or a decrease in polarization, as observed by Tantilla and coworkers.[3] The application of the oscillating electric field may be accompanied by spurious oscillating stray magnetic field, which may produce $\Delta m = \pm 1$ transitions. One can perform the experiment only if one distinguishes the effect of the applied magnetic and electric fields, perhaps by observing the shape of the magnetic induction signal after an initial rf electric field pulse, or by applying the pulse at a frequency where $\Delta m = \pm 1$ transitions are highly improbable or absent.

In summary, the reciprocal Stark effect in spin resonance has been observed in terms of FID electric signals emitted by an ensemble of precessing nuclear-quadrupole moments. After these moments are placed into superposition states by a rf magnetic field pulse, they induce coherent oscillations of atomic polarization in a noncentrosymmetric crystal. The summation of these polarizations over the excess Boltzmann spin population provides macroscopic electric signals from the sample placed between the plates of a capacitor in a tuned circuit. Experiments on the NQR of ^{35}Cl in a $NaClO_3$ single crystal show Zeeman beat patterns for the electric signal which are different from the magnetic FID Zeeman beat patterns. Stray magnetic induction signals are canceled out by a series pickup coil in proximity to the sample, leaving out the electric signal. By proper choice of the orientations of the single crystal of $NaClO_3$ in our experiment we achieved this cancellation because the electric signal vanishes in the absence of a Zeeman field, while the stray magnetic signal remains to be canceled. This procedure was necessary in the case of NQR where the level separation provides a single frequency at which both electric and magnetic signals occur for $\Delta m = \pm 1$ and $\Delta m = \pm 2$ transitions. In high magnetic fields involving systems with more than two levels, one may excite magnetic two photon transitions and thus observe electric signals corresponding to $\Delta m = \pm 2$. This approach should allow for isolation from stray magnetic signals by several orders of magnitude. In this case it appears that measurements of the electric signal from powdered samples would be best carried out.

Although the electric signal is smaller than the magnetic signal, there is in general sufficient signal power to allow measurements at higher temperatures with conventional amplifiers. The signal signature is indicative of the local polarizability of near-neighbor atoms and their structure, and is particularly sensitive to bond angles. The single-crystal Zeeman beat pattern of the NQR-induced electric signal predicts the identification of crystal enantiomorphs, provided one knows the crystal structure and the polarizability of the wave functions. Given the appropriate nucleus and noncentrosymmetric crystal structure, the electric signal can serve as a monitor of local atomic rearrangements and fluctuations—a supplementary source of data to that provided by the effect of electric quadrupole interactions on magnetic signal studies. Phase transitions, charge density waves, or charge carriers produced by means external to the crystal are examples of phenomena that can be studied by the reciprocal Stark electric signal.

ACKNOWLEDGMENTS

We thank T. P. Das, C. J. Grayce, R. A. Harris, A. Pines, K. N. Raymond, H. F. Schaffer, H. L. Strauss, and D. H. Templeton for helpful discussions. This work was supported by the Director, Office of Energy Research, Office of Basic Energy Sciences, Materials Science Division of the U.S. Department of Energy under Contract No. DE-AC03-76SF00098 (M.B.H., C.H., and J.C.) and by the National Science Foundation under Contract No. DMR-83-08082 (T.S. and E.L.H.).

APPENDIX

A quantitative estimate of the electric polarization signal P is made from measurement of the signal at the output of the mixer (see Fig. 1). The induced voltage across the total circuit capacitance is given by $V = PA_s/C$, where A_s is the area of the sample in the sample capacitor (see Fig. 1), and C is the total circuit capacitance. The current $I = V/R_i$ through the SQUID input coil can be written as

$$I = PA_s Q\omega_0 ,$$

where $Q = 1/R\omega_0 C$ is the quality factor of the circuit and ω_0 is the circuit resonant frequency (assumed to be equal to the signal frequency). The circuit Q is measured by injecting a small rf pulse into the circuit through the transmitter coil and recording the ring-down time $\tau = Q/\omega_0$.

The current amplified by the SQUID can be calibrated by making use of the saturation properties of the SQUID.[5] We assume that the voltage across the SQUID is sinusoidal in the input flux so that $V = V_0 \sin(2\pi\Phi/\Phi_0)$. Given an input flux $\phi = \tilde{\Phi}\sin(\omega t)$, where $\tilde{\Phi}$ is a slowly varying function of time, the voltage is $V(t) = V_0 \sin[2\pi\tilde{\Phi}\sin(\omega t)/\Phi_0]$. The amplitude of $V(t)$ at frequency ω is

$$\tilde{V} = \frac{1}{\pi}\int_{-\pi}^{\pi} V_0 \sin[2\pi\tilde{\Phi}\sin(\eta)/\Phi_0]\sin\eta\, d\eta$$

where $\eta = \omega t$. We apply the general rule

$$\sin(z\sin\eta) = 2\sum_{n=1}^{\infty} J_n(z)\sin(n\eta)$$

to obtain

$$\tilde{V} = 2V_0 J_1(2\pi\tilde{\Phi}/\Phi_0) ,$$

where J_n is the nth-order Bessel function. The first maximum occurs at $\tilde{\Phi}=0.29\Phi_0$ and the second minimum is at $\tilde{\Phi}=0.61\Phi_0$. Since $I/\Phi=1/\alpha(L_iL)^{1/2}=1.7\ \mu\text{A}/\Phi_0$ we have $\tilde{I}=(1.7\ \mu\text{A})\tilde{\Phi}/\Phi_0$, where $I=\tilde{I}\sin(\omega t)$; thus the first maximum occurs at $I=0.5\ \mu$A. The following procedure was used to calibrate the input current. A small signal, 0.5 μA peak to peak, was injected into the input circuit through the transmitter coil to produce the first maximum in the SQUID output. The injected signal was reduced by a factor of 10 to 0.05 μA, a current range over which the response of the SQUID is approximately linear.

[1]G. W. Ludwig and H. H. Woodbury, Phys. Rev. Lett. **7**, 240 (1961); A. Abragam and B. Bleaney, *Electron Paramagnetic Resonance of Transition Ions* (Clarendon, Oxford, 1970), pp. 209–216 and 659–664.

[2]N. Bloembergen, in *Proceedings of the XI Colloque Ampere Conference on Electric and Magnetic Resonance, Eindhoven, 1962,* edited by J. Smidt (North-Holland, Amsterdam, 1963), p. 39; F. A. Collins and N. Bloembergen, J. Chem. Phys. **40**, 3479 (1961).

[3]J. W. Culvahouse, David P. Schinke, and Donald L. Foster, Phys. Rev. Lett. **18**, 117 (1967); E. Brun, R. Hann, W. Pierce, and W. H. Tantilla, *ibid.* **8**, 365 (1962).

[4]Tycho Sleator, Erwin L. Hahn, Michael B. Heaney, Claude Hilbert, and John Clarke, Phys. Rev. Lett. **57**, 2756 (1986).

[5]C. Hilbert and J. Clarke, Appl. Phys. Lett. **43**, 694 (1983); IEEE Trans. Magn. **21**, 1029 (1985); J. Low Temp. Phys. **61**, 263 (1985).

[6]R. W. Dixon, in *Proceedings of the XIII Colloque Ampere, Eindhoven, 1964,* edited by L. Van Gerven (North-Holland, Amsterdam, 1965), p. 213; L. Duchesne, M. Read, and P. Cornil, J. Phys. Chem. Solids **24**, 1333 (1963).

[7]R. M. Sternheimer, Phys. Rev. **95**, 736 (1954). An *ab initio* calculation for the Cl—O bond would predict an induced electric dipole moment as well as an enhancement of the Cl nuclear-quadrupole moment.

[8]N. Bloembergen and R. V. Pound, Phys. Rev. **95**, 9 (1954).

[9]M. Bloom and M. A. LeGros, Can. J. Phys. **64**, 1522 (1986).

[10]C. Hilbert, J. Clarke, T. Sleator, and E. L. Hahn, Appl. Phys. Lett. **47**, 263 (1985).

[11]M. Bloom, E. L. Hahn, and B. Herzog, Phys. Rev. **97**, 1699 (1955).

[12]C. P. Slichter, *Principles of Magnetic Resonance,* 2nd ed. (Springer-Verlag, Berlin, 1978), Chap. 9; J. D. Jackson, *Classical Electrodynamics,* 2nd ed. (Wiley, New York, 1975), p. 136; C. Cohen-Tannoudji, B. Diu, and F. Laloe, *Quantum Mechanics* (Wiley-Interscience, New York, 1977), p. 1064. Different authors use different conventions for Q_2^m. The choice of convention is arbitrary provided the expression for the potential [Eq. (8)] is consistent with the definitions of the quadrupole moment operators [Eq. (7)].

[13]W. H. Zachariasen, Z. Kristallogr. Mineral. **71**, 517 (1929); G. N. Ramachandran and K. S. Chandrasekaran, Acta Crystallogr. **10**, 671 (1957); M. E. Burke-Laing and K. N. Trueblood, Acta Crystallogr., Sect. B **33**, 2698 (1977); S. C. Abrahams and J. L. Bernstein, *ibid.* **33**, 3601 (1977).

[14]The sign and magnitude of the induced dipole effect have been calculated quantum mechanically for the HD molecule as a test case. A molecular orbital (MO) calculation at the equilibrium H—D bond distance of 0.74 Å has been carried out by R. A. Harris, C. J. Grayce, and Erwin L. Hahn, Chem. Phys. Lett. **147**, 443 (1988). The dipole moment induced by the D nuclear-quadrupole moment (0.0027 b) in the molecule is evaluated. Numerical results in first order give an induced dipole moment $p=-1.9\times10^{-11}$ D, assuming a time-independent quadrupole interaction due to the Q_2^0 term. In the asymptotic limit of the MO method, extended to the equilibrium bond distance, the induced moment becomes $p=+1.7\times10^{-9}$ D, as expected according to the stick and ball model. Although in this example the quadrupole-induced dipole effect would be too small to measure, it is confirmed that the minus sign for the value of p can be predicted by the MO method as opposite to the sign required by the stick and ball model.

[15]H. Hatanaka, T. Teraar, and T. Hashi, J. Phys. Soc. Jpn. **39**, 835 (1975); D. G. Gold and E. L. Hahn, Phys. Rev. A **16**, 324 (1977).